CORROSION AND PROTECTION OF METALS / КОРРОЗИЯ И ЗАЩИТА МЕТАЛЛОВ

UDC 621.9.048
https://doi.org/10.17073/0021-3438-2024-2-55-69

Research article
Научная статья

Fabrication of high speed steel electrodes with $MoSi_2$–MoB–HfB_2 ceramic additives for electrospark deposition on die steel

A. Akhmetov[1], **Zh.V. Eremeeva**[1], **A.E. Kudryashov**[1], **P.A. Loginov**[1], **S.D. Shlyapin**[2,1], **M.E. Samoshina**[1], **E.A. Levashov**[1]

[1] **National University of Science and Technology "MISIS"**
4 Bld 1 Leninskiy Prosp., Moscow 119049, Russia

[2] **Moscow Aviation Institute (National Research University)**
4 Volokolamskoe shosse, Moscow 125993, Russia

✉ Amankeldy Akhmetov (aman1aotero@gmail.com)

Abstract: The electrodes for electrospark deposition (ESD) were fabricated from hot-pressed blanks composed of a mechanically alloyed powder mixture of R6M5K5 high speed steel. This mixture was enriched with a 40 % addition of heat-resistant $MoSi_2$–MoB–HfB_2 ceramics, produces through the self-propagating high-temperature synthesis method (resulting in the R6M5K5-K electrode), as well as variant without any ceramic addition (resulting in the R6M5K5 electrode). We examined both the composition and structure of the electrode materials and the coatings derived from them, identifying the characteristics of mass transfer from hot-pressed electrodes to substrates of 5KhNM die steel under various frequencies and energy conditions during processing. The R6M5K5 electrode consists of an α-Fe-based matrix incorporating dissolved alloying elements and contains discrete particles of ferrovanadium, tungsten carbide, and molybdenum. The R6M5K5-K electrode, in addition to the α-Fe-based matrix, includes borides and carbides, as well as hafnium oxide. The use of the R6M5K5 electrode resulted in a consistent weight increase in the cathode throughout the entire 10-minute processing period. In contrast, the application of the ceramic-enhanced electrode led to weight gain only during the initial 3 min of processing. Subsequently, ESD produced coatings of 22 and 50 μm thickness on the surface of 5KhNM steel using R6M5K5 and R6M5K5-K electrodes, respectively. The introduction of SHS ceramics escalated the roughness (R_a) of the surface layers from 6 to 13 μm and the hardness from 9.1 to 15.8 GPa. The coating from the R6M5K5 electrode was composed of austenite (γ-Fe) and exhibited high uniformity. Conversely, the coating from the R6M5K5-K electrode consisted of a diverse matrix with both crystalline and amorphous iron, an amorphous phase rooted in the Fe–B alloy, and scattered phases of HfO_2, $HfSiO_4$, Fe_3Si, and Fe_3B. High-temperature tribological testing at 500 °C in an air atmosphere showed that the coatings possess a friction coefficient of 0.55–0.57 when coupled with a counterbody of AISI 440C steel. The integration of heat-resistant ceramics notably enhanced the coating's wear resistance, increasing it by a factor of 13.5.

Keywords: electrospark deposition, powder high speed steel, tool steel, ceramics, silicides, borides, oxides, self-propagating high-temperature synthesis, wear resistance.

Acknowledgments: The study was supported by the Russian Science Foundation grant No. 23-49-00141: https://rscf.ru/project/23-49-00141/

For citation: Akhmetov A., Eremeeva Zh.V., Kudryashov A.E., Loginov P.A., Shlyapin S.D., Samoshina M.E., Levashov E.A. Fabrication of high speed steel electrodes with $MoSi_2$–MoB–HfB_2 ceramic additives for electrospark deposition on die steel. *Izvestiya. Non-Ferrous Metallurgy*. 2024;30(2):55–69. https://doi.org/10.17073/0021-3438-2024-2-55–69

Получение электрода из быстрорежущей стали с керамической добавкой $MoSi_2$–MoB–HfB_2 для электроискровой обработки штамповой стали

А. Ахметов[1], Ж.В. Еремеева[1], А.Е. Кудряшов[1], П.А. Логинов[1], С.Д. Шляпин[2,1], М.Е. Самошина[1], Е.А. Левашов[1]

[1] **Национальный исследовательский технологический университет «МИСИС»**
Россия, 119049, г. Москва, Ленинский пр-т, 4, стр. 1

[2] **Московский авиационный институт (национальный исследовательский университет)**
Россия, 125993, г. Москва, Волоколамское шоссе, 4

✉ Аманкельды Ахметов (aman1aotero@gmail.com)

Аннотация: Получены электроды для электроискровой обработки (ЭИО) из горячепрессованных заготовок механически легированной порошковой смеси быстрорежущей стали марки Р6М5К5 с 40 %-ной добавкой жаростойкой керамики $MoSi_2$–MoB–HfB_2, полученной методом самораспространяющегося высокотемпературного синтеза (электрод марки Р6М5К5-К), и без добавки (электрод Р6М5К5). Изучены состав и структура электродных материалов и сформированных из них покрытий. Определены особенности массопереноса горячепрессованных электродов на подложках из штамповой стали 5ХНМ при варьировании частотно-энергетических режимов обработки. Электрод Р6М5К5 состоит из матрицы на основе α-Fe, в которой растворены легирующие элементы, и нерастворенных частиц феррованадия, карбида вольфрама и молибдена. Электрод Р6М5К5-К содержит матрицу на основе α-Fe, бориды и карбид, а также оксид гафния. При использовании электрода Р6М5К5 наблюдался устойчивый привес на катоде за все 10 мин обработки. В случае электрода с добавкой керамики привес отмечался в первые 3 мин легирования. В результате ЭИО на поверхности стали 5ХНМ были сформированы покрытия толщиной до 22 и 50 мкм для Р6М5К5 и Р6М5К5-К соответственно. Введение СВС-керамики способствовало росту шероховатости (R_a) поверхностных слоев с 6 до 13 мкм и твердости с 9,1 до 15,8 ГПа. Покрытие из электрода Р6М5К5 состояло из аустенита (γ-Fe) и характеризовалось высокой однородностью. Покрытие из электрода Р6М5К5-К представляло собой гетерогенную матрицу на основе кристаллического и аморфного железа, аморфной фазы на основе сплава Fe–B и дисперсных фаз HfO_2, $HfSiO_4$, Fe_3Si и Fe_3B. Высокотемпературными трибологическими испытаниями при температуре 500 °С на воздухе выявлено, что покрытия обладают коэффициентом трения 0,55–0,57 в паре с контртелом из стали AISI 440C, а введение добавки жаростойкой керамики способствовало увеличению износостойкости покрытия в 13,5 раза.

Ключевые слова: электроискровая обработка, легирование, порошковая быстрорежущая сталь, инструментальная сталь, керамика, силициды, бориды, оксиды, самораспространяющийся высокотемпературный синтез, износостойкость.

Благодарности: Исследование выполнено за счет гранта Российского научного фонда № 23-49-00141,
https://rscf.ru/project/23-49-00141/

Для цитирования: Ахметов А., Еремеева Ж.В., Кудряшов А.Е., Логинов П.А., Шляпин С.Д., Самошина М.Е., Левашов Е.А. Получение электрода из быстрорежущей стали с керамической добавкой $MoSi_2$–MoB–HfB_2 для электроискровой обработки штамповой стали. *Известия вузов. Цветная металлургия*. 2024;30(2):55–69.
https://doi.org/10.17073/0021-3438-2024-2-55–69

Introduction

During operation, die tools subjected to high temperatures face rapid wear and crack propagation due to thermal effects, friction, adhesion, and micro-cracks, among other causes [1—4]. Consequently, tools require frequent replacement, leading to workflow disruptions and significant economic costs.

Electrospark deposition (ESD) of wear-resistant coatings using various electrode materials has proven to be an effective method to restrain rapid wear and extend the service life of die tools [5; 6]. These materials include graphite [7; 8], metals [9; 10], alloys [11; 12], ceramics [13; 14], and hard alloys [15; 16]. The broad spectrum of electrode materials available allows for the selection of an appropriate composition to tailor the coating for a specific functional requirement. Furthermore, the application of high-energy modes expands the capabilities of the method, facilitating the restoration of worn tool surfaces [17]. The production of electrodes by consolidating powdered components enables the incorporation of the aforementioned materials, which are often runoff products, thereby significantly improving the prospects for industrial application [18—21].

Wear-resistant and heat-resistant electrode materials are essential for hardening the surfaces of dies operating at elevated temperatures. In this context, heterophase ceramic composite $MoSi_2$—MoB—HfB_2, derived from self-propagating high-temperature synthesis (SHS), merits particular attention due to its highly homogeneous component distribution within the mixture [22; 23]. Although electrospark coatings produced from this ceramic are extremely hard and heat-resistant—an important attribute for hardening high-temperature tools—they are also characterized by a low deposition rate and inadequate wear resistance in high-temperature tribological tests [23]. To improve mass transfer in the discharge arc and to bolster the wear resistance of the coatings, cermet electrodes, comprising a metallic binder and a refractory component, are employed. High speed steel (HSS), known for its red-hardness (the ability to maintain hardness at elevated temperatures) and high wear resistance, is a suitable choice for the binder [24; 25]. Additionally, the use of HSS not only enhances wear resistance at high temperatures but also reduces costs and streamlines the electrode production process by lowering the sintering temperature.

The aim of this study was to fabricate electrodes from hot-pressed blanks of mechanically alloyed powder mixture of R6M5K5 high speed steel with $MoSi_2$—MoB—HfB_2 ceramics, and to investigate the characteristics of electrospark coating formation on 5KhNM die steel.

Materials and methods

The widely used R6M5K5 steel was selected as the binder. It was fabricated in the Activator-4M planetary ball mill (PBM) (CJSC "Activator", Novosibirsk) from elemental powders by mixing Fe, W, Mo, Co, Cr, C, and ferrovanadium FVd50U0.5 (FVd) with the following ratio, wt.%: 6.0 W; 5.0 Mo; 5.0 Co; 4.0 Cr; 0.9 C; 4.0 FVd (2.0 V); with the remainder being Fe. The characteristics of the powders are presented in Table 1.

The components were mixed for 30 minutes with the drums rotating at a rate of 800 rpm. The main fraction of finished HSS mixture exhibited a grain size of 3—20 μm, with an average particle size of 10 μm.

Heterophase ceramics with a composition of 60 % (90%$MoSi_2$—10%MoB) plus 40 % HfB_2 were synthesized using the method outlined in [22]. The SHS sintered material was pulverized in a rotary ball mill to produce a powder with a particle size of less than 40 μm. This powder, constituting 40 % of the mix, was combined with the HSS powder in a PBM Pulverisette 5/2 ("Fritsch", Germany) for 60 minutes, with the drums rotating at a speed of 300 rpm.

The final composition of the powder mixture was as follows, wt.%: 3.6 W; 3.0 Mo; 3.0 Co; 2.4 Cr; 0.54 C; 1.2 V; 21.6 $MoSi_2$; 2,4 MoB; 16.0 HfB_2; the remainder being Fe.

Blanks made of R6M5K5 steel (R6M5K5 electrode) and the HSS mixture with heterophase ceramics (R6M5K5-K electrode) were produced by hot pressing (HP) at a temperature of 1000 °C, under a pressure of 50 MPa, with a holding time of 3 minutes using the DSP-515 SA press ("Dr. Fritsch Sondermaschinen GmbH", Germany) in a graphite mold of 50 mm diameter. Electrodes measuring 20—50 mm in length and having a cross-section of 5×5 mm were fashioned by wire electrical discharge machining of the hot-pressed blanks on the ARTA 200-2 EDM machine (JSC "Scientific Industrial Corporation Delta-Test", Fryazino).

The ESD process was performed using Alier-Metal 30 and Alier-Metal G53 setups (SPA "Metal" LLC —

Table 1. **Characteristics of powders used in the preparation of the R6M5K5 powder mixture**

Таблица 1. Характеристики порошков, использованных для получения порошковой смеси Р6М5К5

Powder brand	Element	GOST/TS	Particle size, μm	Purity, %
PZhRV 2.200.26	Fe	TS 14-5365-98	<120	99.24
PVCh	W	TS 48-19-57-91	1–5	99.99
PMCh	Mo	TS 14-22-160-2002	40–60	99.90
PK-1	Co	GOST 9721-79	<50	99.95
ERKh-1	Cr	GOST 5905-2004	<50	99.99
FVd50U0.5	V	GOST 27130-94	<50	99.00
P-803	C	GOST 7885-86	<20	99.90

Table 2. **ESD process parameters**

Таблица 2. Параметры процесса ЭИО

Mode	Setup	Pulsed discharge current rate, A	Recurrence rate, Hz	Pulse duration, μs	Single-pulse energy, J	Total energy ΣE, kJ·min
1	Alier-Metal 30	170	1500	25	0.1	7.65
2	Alier-Metal 30	170	3000	25	0.1	15.30
3	Alier Metal G53*	200	400	100	0.4	9.60

* Auxiliary generator.

SCINTI S.R.L., Russia — Moldova) under varying frequency and energy treatment conditions, the specifics of which are detailed in Table 2.

The deposition of the coating was achieved through the alternating localized impact of pulsed discharge on all areas of the processing surface of 5KhNM steel samples. This was done by having the anode repeatedly pass over the same cathode area in an argon environment.

The kinetics of mass transfer — specifically, the anode erosion (ΔA_i) and the cathode's specific weight gain (ΔK_i) — for the R6M5K5 and R6M5K5-K electrodes was determined using a gravimetric method on a KERN 770 analytical balance (KERN, Germany) with an accuracy of 10^{-5} g. The electrodes were weighed after treating an area of 1 cm^2 for 1 minute, with the treatment continuing for a total of 10 minutes. The total cathode weight gain, SDKi, was calculated using the formula [26]:

$$\Sigma \Delta K_i = \Delta K_1 + \Delta K_2 + ... + \Delta K_{10}, \qquad (1)$$

where ΔK_i is the cathode weight gain for the i-th minute of alloying, g; $i = 1, 2, ..., 10$.

The total anode erosion $\Sigma \Delta A_i$ was calculated similarly.

The microstructure of the fabricated electrodes and coatings was examined using a S-3400N scanning electron microscope (SEM) ("Hitachi High-Technologies Corporation", Japan), equipped with a NORAN System 7 energy-dispersive spectrometer for *X*-ray microanalysis ("Thermo Scientific", USA).

X-ray diffractometric (XRD) phase analysis of the electrodes was conducted using a DRON-4 diffractometer (Research and Production Enterprise "Bourevestnik", St. Petersburg) with CoK_α radiation. For the XRD analysis of electrospark coatings, a D2 PHASER diffractometer ("Bruker AXS GmbH", Germany) with monochromatic CoK_α radiation was utilized.

The surface topography of the coatings and the profiles of the wear tracks were analyzed using a WYKO NT 1100 optical profilometer (VEECO, USA).

Hardness measurements on cross-sections were performed using the method of instrumented indentation with a NanoHardness Tester ("CSM Instruments", Switzerland), in accordance with GOST R 8.748-2011 (ISO 14577).

Tribological testing of the coatings was carried out in accordance with the ASTM G 99 standard, employing a pin-on-disk configuration on a High-Temperature Tribometer ("CSM Instruments", Switzerland). A 6 mm diameter ball made of AISI 440C steel (equivalent to 95X18) served as the counterbody. The test conditions were as follows: temperature at 500 °C, load at 5N, linear velocity at 10 cm/s, counterbody path length at 500 m, and track length at 3.76 cm.

Wear resistance (W) was calculated using the formula:

$$W = SL/(Hl), \qquad (2)$$

where S is the cross-sectional area of the groove wear, mm^2; L is the track length, mm; H is the load, N; and l is the friction path, m.

The microstructure of the lamella from the coating deposited by the R6M5K5-K electrode was examined using a JEM-2100 microscope ("Jeol", Japan) employing high-resolution transmission electron microscopy (HR TEM). The lamella samples were prepared using a focused ion beam tool (Quanta 200 3D FIB Instrument, FEI Company, USA). *In situ* observations were also conducted within the transmission electron microscope column at a temperature of 500 °C.

Results and discussion

Characteristics of electrodes

The outcomes of the XRD analysis for the R6M5K5-K electrode are detailed in Table 3. Analysis reveals that the electrode comprises an α-Fe-based matrix, borides including $(Mo,W)_2FeB_2$, Mo_3CoB_3, and HfB, Mo_6Fe_6C carbide, and hafnium oxide. A notable decrease in the lattice constant of the α-Fe phase was observed, indicative of silicon dissolution. This dissolution is likely to significantly reduce the α-Fe lattice constant [27], a finding that aligns with the elemental distribution maps shown in Fig. 1.

According to the SEM and EDS data (Table 4) for the R6M5K5-K electrode, the identified structural components include HfB hafnium monoboride; an iron-based phase (α-Fe) containing dissolved alloying elements from the HSS itself as well as silicon from the heterophase ceramics; and a complex carbide of iron and molybdenum, Mo_6Fe_6C.

Figure 2 displays the SEM image showing the microstructure of the electrode composed of HSS R6M5K5, alongside the element distribution map. The image reveals that the Fe-based matrix is made up of grains ranging from 1 to 2 μm, within which alloying elements (Co and Cr) are uniformly dissolved. The matrix contains particles of different colors; based on the EDS data and the element distribution map, it's determined that the lighter particles are tungsten carbide (WC), produced through mechanical alloying, whereas the darker par-

Table 3. **Phase composition of R6M5K5-K electrode**

Таблица 3. Фазовый состав электрода Р6М5К5-К

Phase	Content		Lattice constant, nm
	vol.%	wt.%	
α-Fe	48.4	44.8	a = 0.2844
$(Mo,W)_2FeB_2$	23.9	23.9	a = 0.55731 c = 0.3136
Mo_6Fe_6C	17.2	18.3	a = 1.1022
Mo_3CoB_3	2.6	2.7	–
HfO_2	5.2	6.1	–
HfB	2.2	3.3	a = 0.4568

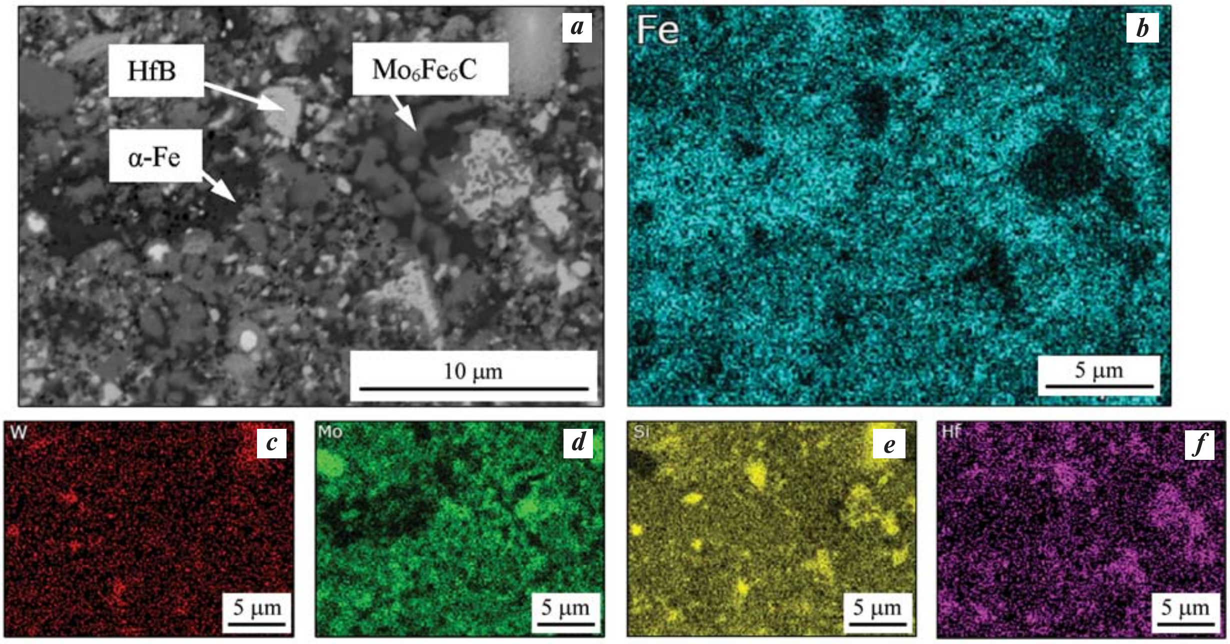

Fig. 1. SEM image of the microstructure of R6M5K5-K electrode (***a***) and the element distribution map: Fe (***b***), W (***c***), Mo (***d***), Si (***e***), and Hf (***f***)

Рис. 1. РЭМ-изображение микроструктуры электрода Р6М5К5-К (***a***) и карта распределения элементов: Fe (***b***), W (***c***), Mo (***d***), Si (***e***) и Hf (***f***)

Table 4. **Chemical composition (at.%) of structural components in the R6M5K5-K electrode**

Таблица 4. Химический состав (ат.%) структурных составляющих электрода Р6М5К5-К

Phase	C	O	Si	V	Cr	Co	Fe	Mo	Hf	W
HfB*	–	–	0.4	3.3	0.5	–	11.4	15.4	69.0	–
α-Fe	–	6.2	20.9	1.6	1.3	3.3	62.5	3.6	–	0.6
Mo_6Fe_6C	47.9	–	9.4	1.5	1.7	1.7	22.1	15.2	–	0.2

* The phase was determined based on the XRF results.

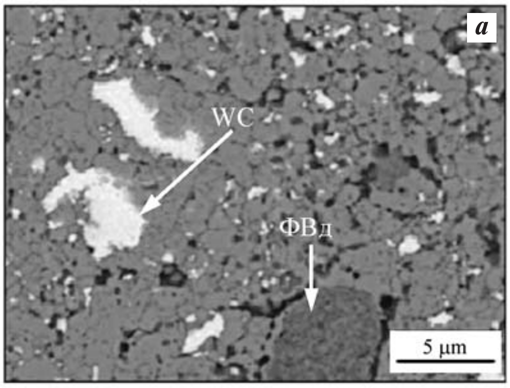

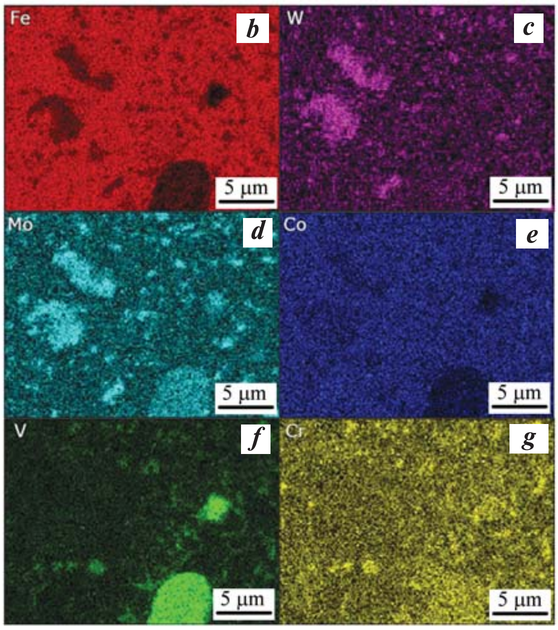

Fig. 2. SEM image of the microstructure of R6M5K5 electrode (***a***) and the element distribution map: Fe (***b***), W (***c***), Mo (***d***), Co (***e***), V (***f***) and Cr (***g***)

Рис. 2. РЭМ-изображение микроструктуры электрода Р6М5К5 (***a***) и карта распределения элементов: Fe (***b***), W (***c***), Mo (***d***), Co (***e***), V (***f***) и Cr (***g***)

ticles are identified as ferrovanadium (FVd). Both WC particles and the undissolved FVd include molybdenum, which is known to form a continuous range of solid solutions with tungsten (W) and vanadium, suggesting a complex interplay of these elements within the electrode's microstructure [28; 29].

Preparation and properties of electrospark coatings

Figure 3 illustrates the effect of the ESD duration using R6M5K5 and R6M5K5-K electrodes on both cathode weight gain and anode erosion. The use of the R6M5K5 electrode leads to a consistent increase in cathode weight alongside similar rates of electrode erosion. A significant correlation was found between the increase in total pulse energy and the weight gain of the substrate, making mode 2 (ΣE = 15.30 kJ·min) the preferred option for the R6M5K5 electrode due to it resulting in the greatest weight gain over a 10-minute deposition period.

Conversely, for the R6M5K5-K electrode, all tested modes yield nearly identical cathode weight gains, which plateau after the first 3 minutes of deposition. The limitation in coating thickness can be attributed to the buildup of internal stresses, a decrease in the thermal resistance of the coating, and the development of an ultra-dispersed structure within it [26].

For the purpose of visually examining the surface topography, the surface roughness (R_a) of the coatings deposited over 3 minutes for each of the three modes was measured. Figure 4 presents 3D images of these surfaces along with their R_a values. It is evident that the use of the R6M5K5 electrode results in a slightly lower surface roughness compared to the R6M5K5-K electrode. The analysis of mass transfer and roughness kinetics indicates that mode 2 is the most favorable. This mode achieves the lowest roughness while ensuring high mass transfer for the R6M5K5 electrode and moderate mass transfer for the R6M5K5-K electrode.

The coatings applied using mode 2 were examined via scanning electron microscopy (SEM). Figures 5 and 6 illustrate the surface topography and the cross-sectional structure of the coating-substrate interface, respectively.

Figure 5 demonstrates that the coating deposited from R6M5K5 electrode without ceramics represents overlaying of spreading drips of melt formed in the pulsed discharge arc. There are almost no cracks in the coating and micropores are detected in the surface layer. The coating is 20—22 μm thick and the transition layer is 5—6 μm. According to the XRD data, along with EDS (Table 5), the coating deposited from R6M5K5 electrode consists of γ-Fe. Austenite (γ-Fe) is formed due to high rates of melt crystallization from the electrode material, which is practically a hardening operation [17]. Ni, Si and Mn are present in the transition layer and form part of the substrate.

Based on the XRD data, the coating deposited from the R6M5K5-K electrode is composed of various phases: α-Fe, HfO_2, $HfSiO_4$, Fe_3Si, and Fe_3B. It is suggested that hafnium silicate $HfSiO_4$ forms in the discharge arc, a result of the reaction between hafnium oxide (present in the electrode) and silicon oxide SiO_2. The silicon oxide likely forms from the oxidation of silicon by impurity oxygen present in the environment.

The use of the R6M5K5-K metal-ceramic electrode leads to increased surface roughness and heterogeneity in the coating's structure. According to the results

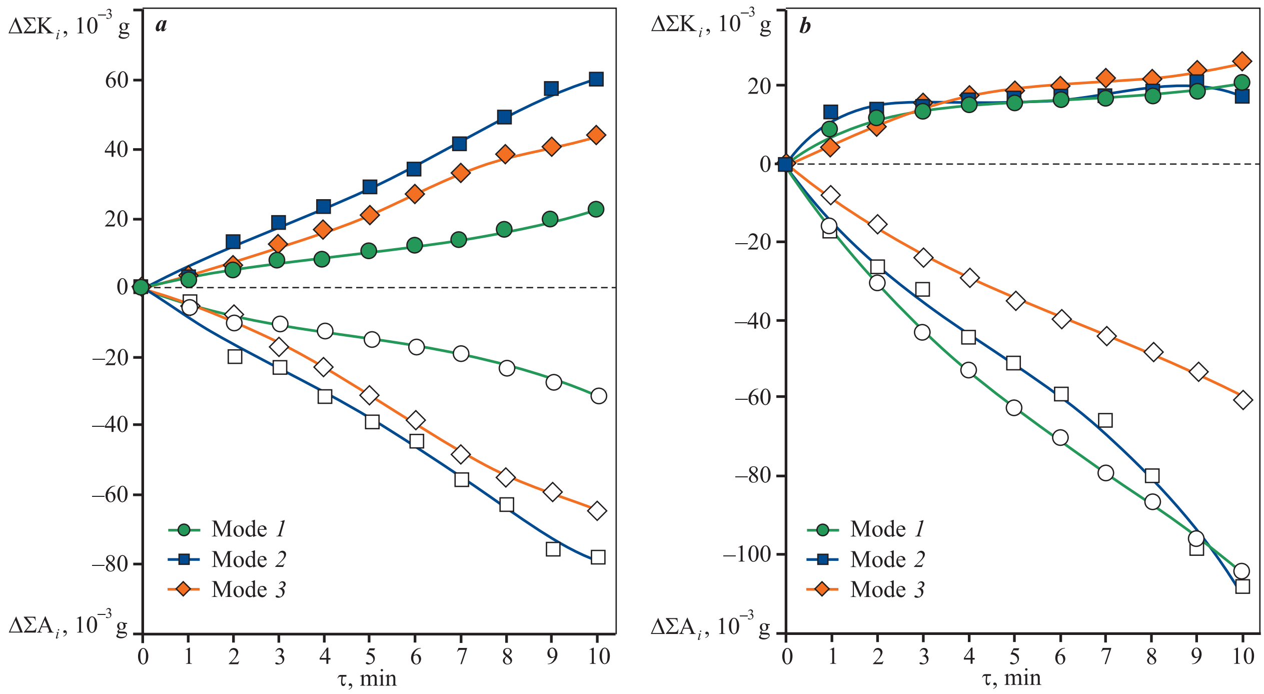

Fig. 3. Dependence of the mass gain of the cathode ($\Delta\Sigma K_i$) and the erosion of the anode ($\Delta\Sigma A_i$) on the duration of ESD of 5KhNM steel with R6M5K5 (***a***) and R6M5K5-K (***b***) electrodes

Рис. 3. Зависимости привеса массы катода ($\Delta\Sigma K_i$) и эрозии анода ($\Delta\Sigma A_i$) от длительности электроискровой обработки стали 5ХНМ электродами Р6М5К5 (***a***) и Р6М5К5-К (***b***)

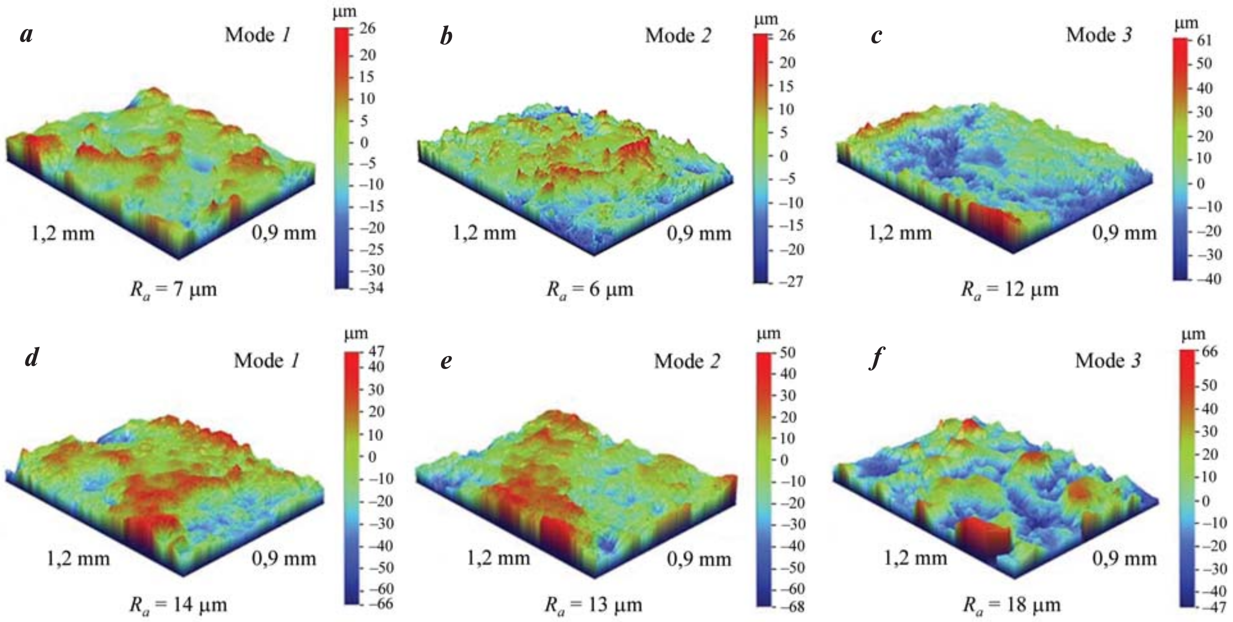

Fig. 4. Surface topography and roughness of coatings deposited from R6M5K5 (***a–c***) and R6M5K5-K (***d–f***) electrodes in ESD modes *1* (***a***, ***d***), *2* (***b***, ***e***), and *3* (***c***, ***f***)

Рис. 4. Топография поверхности и шероховатость покрытий из электродов Р6М5К5 (***a–c***) и Р6М5К5-К (***d–f***) на ЭИО-режимах *1* (***a***, ***d***), *2* (***b***, ***e***), *3* (***c***, ***f***) of EDS analysis presented in Table 6, which analyzed different areas of the coating as marked in Fig. 6, *b*, the thickness of the coating varies between 20 and 30 μm, with some areas reaching up to 50 μm. Under high magnification, a fine-grained microstructure is visible, with grain sizes ranging from 0.3 to 0.6 μm. Additionally, a dendritic structure, reminiscent of eutectics, is also observed alongside dispersed inclusions smaller than 0.1 μm. The iron-based matrix incorporates dissolved alloying elements from both the steel and the ceramic additive.

The submicron and nanosized structural components of the coating were analyzed using the transmission electron microscopy method (TEM). Figure 7 showcases SEM images of the lamella before (Fig. 7, *a*) and after (Fig. 7, *c*) heating to 500 °C. Additionally, diffraction patterns of sections of the α-Fe-based matrix (Fig. 7, *b*) and the Fe—B-based amorphous phase (Fig. 7, *d*) are displayed. The specific area from which the lamella was extracted is indicated in Fig. 6, *b*.

Using SEM (Fig. 7) and EDS analysis (Table 7) we characterized the composition of an α-Fe-based crystalline matrix interspersed with amorphous inclusions of a similar composition. These amorphous inclusions arose both from the rapid cooling associated with the ESD process and the presence of amorphizing elements such as boron and silicon [30; 31]. Furthermore, we identified an Fe—B amorphous phase containing inclusions of Fe_3B iron boride nanoparticles. These nanoparticles are released upon heating as the amorphous matrix segregates into Fe_3B and α-Fe [32]. Distributed throughout the matrix volume are nanoparticles of HfO_2, measuring 30—50 nm, and iron silicide Fe_3Si, which are 15—20 nm in size.

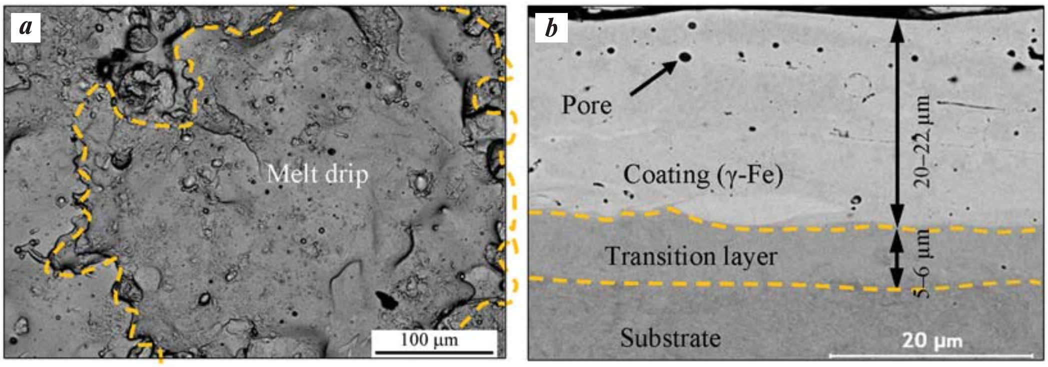

Fig. 5. SEM images of the topography (***a***) and structure (***b***) of the coating (mode *2*) deposited from R6M5K5 electrode

Рис. 5. РЭМ-изображения топографии (***а***) и структуры (***b***) покрытия (режим *2*) из электрода Р6М5К5

Table 5. **Chemical composition (at.%) of various areas within the coating deposited from R6M5K5 electrode**

Таблица 5. Химический состав (ат.%) областей покрытия, полученного электродом Р6М5К5

Area of analysis	C	Si	V	Cr	Mn	Fe	Co	Ni	Mo	W
Coating	15.0	–	2.2	2.0	–	74.5	3.0	–	1.8	1.4
Transition layer	9.4	0.6	–	0.7	1.0	86.8	0.0	1.6	–	0.1
Substrate	10.3	0.6	–	0.8	0.7	86.1	0.0	1.4	–	–

Table 6. Chemical composition (at.%) of the coating areas marked in Fig. 6, *b*

Таблица 6. Химический состав (ат.%) областей покрытия, отмеченных на рис. 6, *b*

Area	C	O	Si	V	Cr	Mn	Fe	Ni	Mo	Hf
1	–	66.3	–	–	–	–	1.9	–	–	31.8
2	16.2	–	13.9	1.4	1.5	–	59.0	–	6.4	1.5
3	23.8	34.1	5.5	1.2	1.4	–	25.8	–	6.8	1.4
4	24.4	40.8	4.5	0.7	–	0.4	25.7	–	3.3	0.2
5	11.6	–	0.8	–	0.5	0.8	84.7	1.5	–	–

Table 7. **Chemical composition (at.%) of the areas marked in Fig. 7, *a***

Таблица 7. Химический состав (ат.%) областей, отмеченных на рис. 7, *a*

Area	Component	Fe	W	Mo	Hf	Si	Cr	V	Co	O
1	Crystal matrix	84.7	1.2	4.0	–	4.8	1.4	0.5	2.0	–
2	Amorphous matrix	87.5	1.0	4.0	–	4.2	1.4	0.5	1.4	–
3	Particle based on HfO_2	4.6	–	–	31.0	–	–	–	–	64.4
4	Fe–B amorphous phase*	21.7	–	–	–	–	–	–	–	78.3

* The phase was determined based on the diffraction pattern.

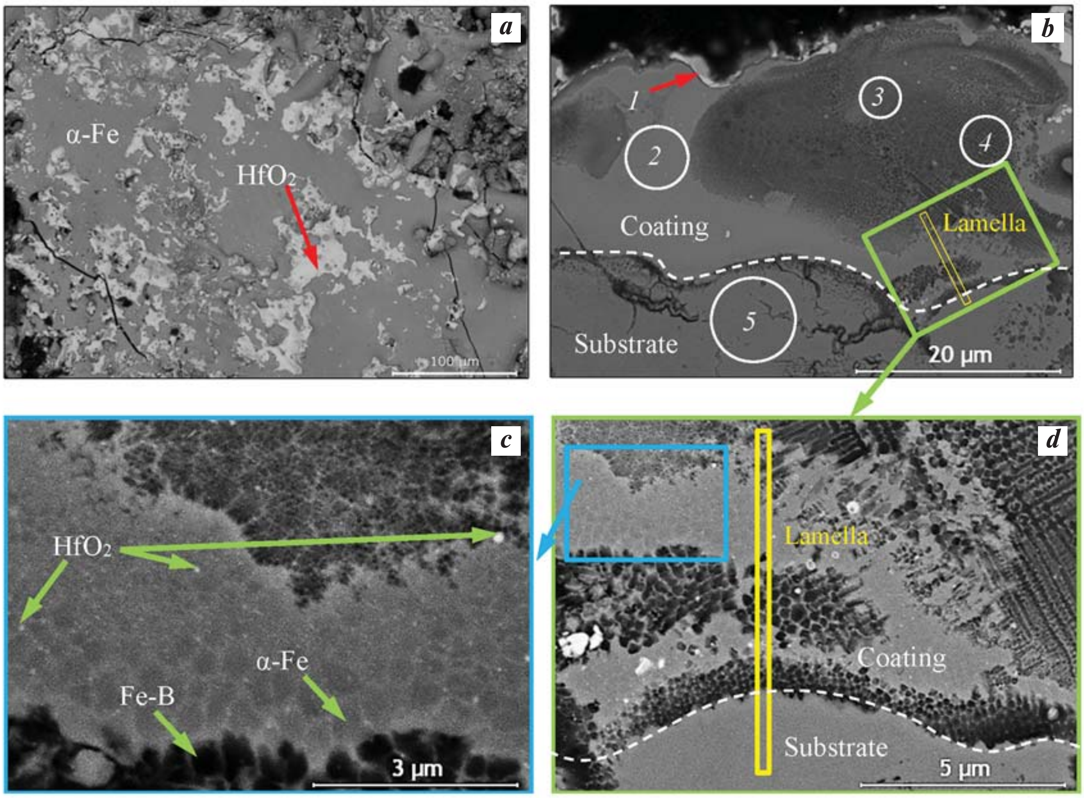

Fig. 6. SEM images of the surface topography (***a***) and the microstructure (***b***–***d***) of the coating deposited from R6M5K5-K electrode

Рис. 6. РЭМ-изображения топографии поверхности (***a***) и микроструктуры (***b***–***d***) покрытия, полученного из электрода Р6М5К5-К

The results from nanoindentation measurements of electrospark coatings deposited from R6M5K5 and R6M5K5-K electrodes were analyzed, and hardness distributions across the coating thickness are illustrated in Fig. 8. It is noticeable that the hardness of the coating deposited from the R6M5K5-K electrode is 15.8±0.4 GPa, which is significantly higher than the 9.1±0.4 GPa hardness of the coating deposited from the R6M5K5 electrode. This increase in hardness is attributed to the inclusion of hardening phases such as HfO_2, $HfSiO_4$, Fe_3B, Fe_3Si within the coating.

High-temperature tribological tests

A critical attribute for tools used in isothermal forging is their wear resistance under conditions of high-temperature friction. While tribological tests conducted according to standard methodologies may not perfectly replicate the actual operating conditions of dies, the results are nevertheless indicative of the impact of the coatings on wear resistance.

Figure 9 illustrates the relationship between the friction coefficient of 5KhNM steel samples with

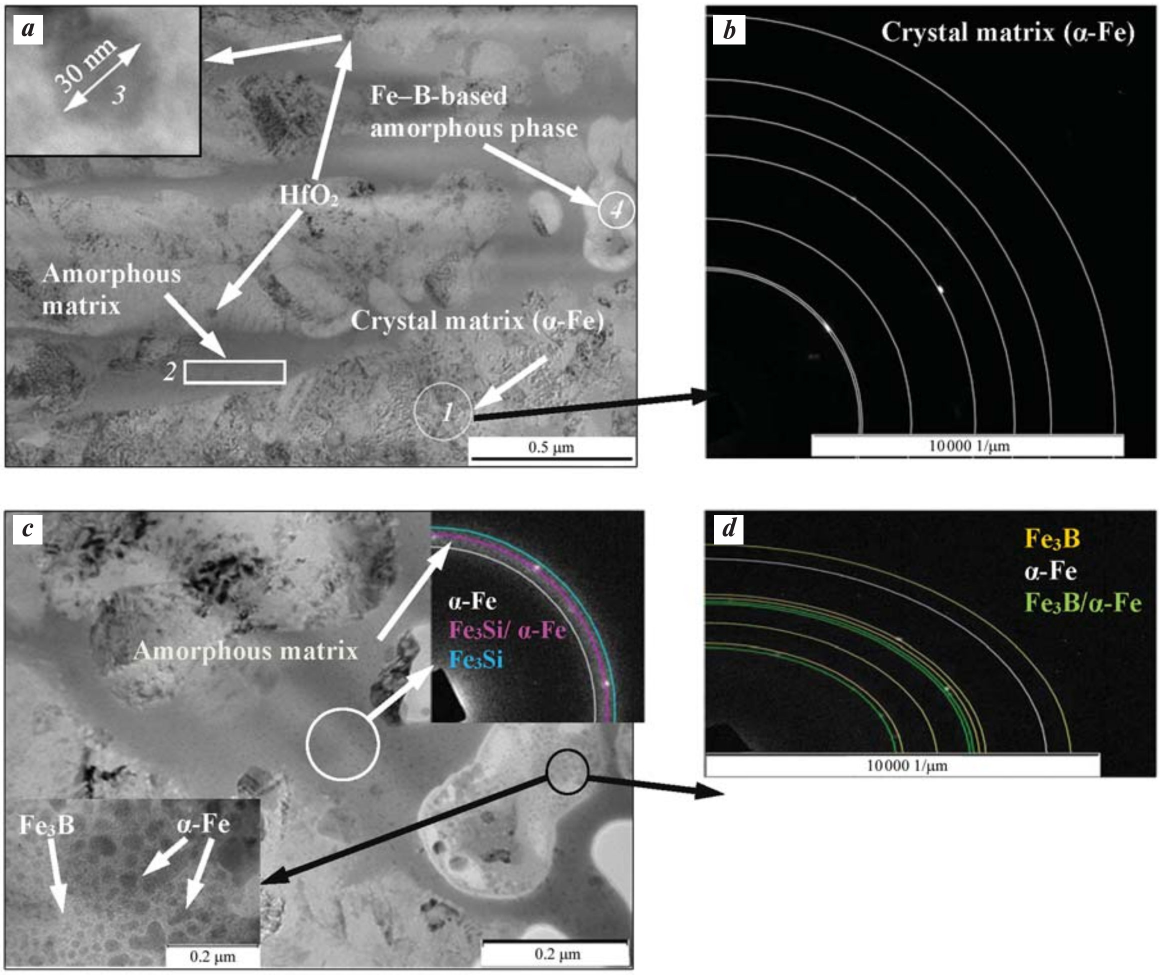

Fig. 7. TEM images of the coating deposited from R6M5K5-K electrode before (***a***) and after (***c***) heating the lamella to 500 °C, diffraction pattern of α-Fe-based matrix (***b***) and Fe–B-based amorphous phase after heating (***d***)

Рис. 7. ПЭМ- изображения покрытия из электрода Р6М5К5-К до (***a***) и после (***c***) нагрева ламели до 500 °С, а также дифракционная картина матрицы на основе α-Fe (***b***) и аморфной фазы Fe–B после нагрева (***d***)

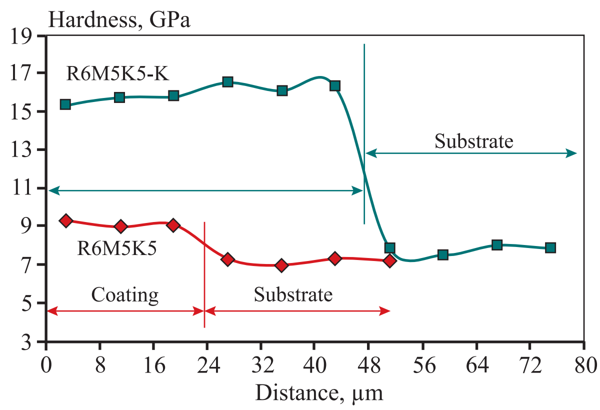

Fig. 8. Hardness distribution over the thickness of electrospark coatings deposited with R6M5K5 and R6M5K5-K electrodes

Рис. 8. Распределение твердости по толщине электроискровых покрытий из электродов Р6М5К5 и Р6М5К5-К

coatings and the counterbody path length at a temperature of 500 °C, along with 2D images of wear track profiles.

Although the friction coefficients for both coatings are similar, ranging from 0.55 to 0.57, the values of reduced wear show significant differences: $38.24 \cdot 10^{-5}$ mm^3/N/m for the coating from R6M5K5 electrode and $2.82 \cdot 10^{-5}$ mm^3/N/m for the coating from R6M5K5-K electrode. This disparity signifies a substantial increase in wear resistance by 13.5 times for the coating containing hardening phases HfO_2, $HfSiO_4$, Fe_3B, and Fe_3Si.

However, a minor fluctuation in the initial path section (20—150 m) for coatings deposited from the R6M5K5-K electrode can be attributed to the counterbody wearing in and the removal of protruding areas of the rough surface (R_a = 13 µm). Additionally,

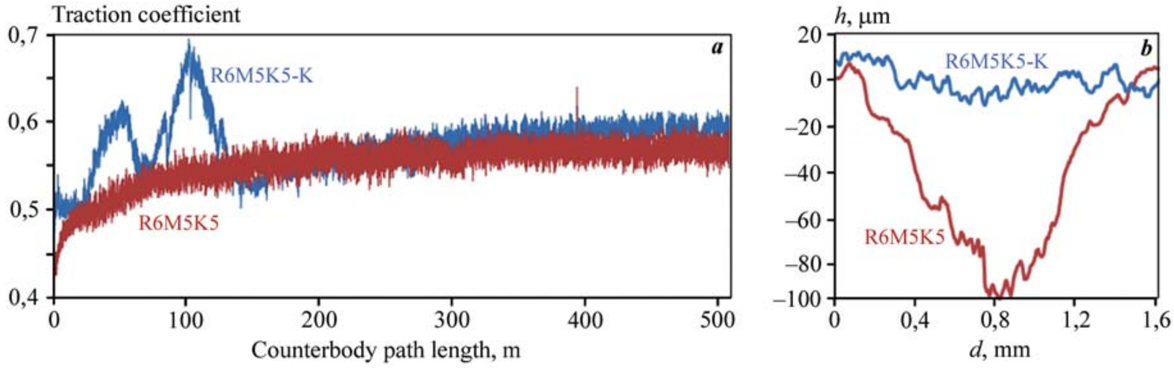

Fig. 9. Dependence of the friction coefficient of electrospark coatings deposited from R6M5K5 and R6M5K5-K electrodes on the sliding distance of the counterbody at 500 °C (***a***) and 2D profiles of wear tracks (***b***)

Рис. 9. Зависимость коэффициента трения электроискровых покрытий из электродов Р6М5К5 и Р6М5К5-К от длины пробега контртела при температуре 500 °С (***a***) и 2D-профили дорожек износа (***b***)

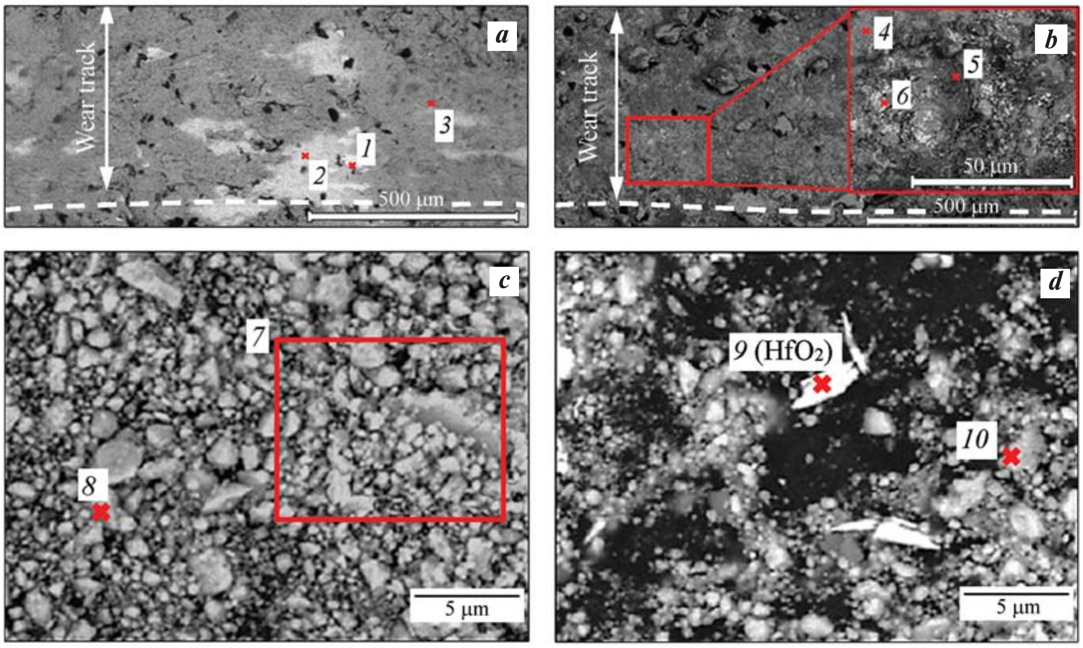

Fig. 10. SEM images of tracks (***a***, ***b***) and wear products (***c***, ***d***) during the tests of electrospark coatings deposited from R6M5K5 (***a***, ***c***) and R6M5K5-K (***b***, ***d***) electrodes

Рис. 10. РЭМ-изображения дорожек (***a***, ***b***) и продуктов износа (***c***, ***d***) при испытаниях электроискровых покрытий, полученных из электродов Р6М5К5 (***a***, ***c***) и Р6М5К5-К (***b***, ***d***)

the chipping of HfO_2 particles during the tests, as confirmed by their presence in the wear products (illustrated in Fig. 10 and Table 8), contributes to this fluctuation.

Oxidation of the components is observed in both coating formulations. As the coating deposited from the R6M5K5 electrode wears off, layers of the coating that are less oxidized become exposed and emerge on the surface. In contrast, the coating deposited from the R6M5K5-K electrode remains quite homogeneous, exhibiting less pronounced wear traces.

Conclusions

1. Electrode materials suitable for the electrospark deposition on die steel were sourced from a powdered mixture of R6M5K5 high speed steel and a powdered mixture of R6M5K5 high speed steel with 40 % boride-silicide ceramics ($MoSi_2$—MoB—HfB_2). Through the examination of mass transfer and roughness kinetics, the optimal processing mode for 5KhNM die steel was identified, which ensures the lowest surface roughness while maintaining acceptable mass transfer rates.

Table 8. **Chemical composition (at.%) of areas in Fig. 10**
Таблица 8. Химический состав (ат.%) областей на рис. 10

Area	O	Si	V	Cr	Fe	Co	Mo	W	Hf
Wear tracks (Fig. 10, *a*, *b*)									
1	27.2	–	2.1	2.2	61.3	3.5	2.1	1.5	–
2	41.3	–	1.6	2.0	48.9	3.3	1.7	1.3	–
3	55.4	–	0.3	0.5	42.7	0.9	–	–	–
4	27.2	13.7	1.6	2.0	41.0	2.9	7.9	0.8	2.9
5	55.4	3.8	0.3	5.9	31.5	0.6	1.4	–	1.1
6	59.6	–	0.7	0.8	15.2	0.6	2.8	–	20.2
Wear products (Fig. 10, *c*, *d*)									
7	54.0	0.8	–	3.6	41.0	–	0.6	–	–
8	42.7	–	1.5	1.5	50.8	–	1.9	1.6	–
9	45.2	5.4	0.7	3.5	28.7	–	2.1	–	14.4
10	47.1	9.7	0.7	1.5	32.4	1.0	3.3	–	4.3

2. The coating applied from R6M5K5 electrode, consisting of austenite, measures 20—22 μm in thickness and is noted for its high uniformity, with a hardness of approximately 9.1±0.4 GPa. On the other hand, the coating from the R6M5K5-K electrode, which incorporates ceramics, features a uniform distribution of hardening phases such as HfO_2, $HfSiO_4$, Fe_3Si, and Fe_3B, and varies in thickness from 20 to 30 μm, achieving a hardness of 15.8±0.4 GPa. The dispersed HfO_2 particles are sized between 30—50 nm, while Fe_3Si particles range from 15—20 nm.

3. High-temperature tribological testing revealed that the coating from the R6M5K5-K electrode exhibits significantly enhanced wear resistance, being 13.5 times greater than that of the coating from the R6M5K5 electrode. The reduced wear rate for the ceramic-enhanced coating was measured at $2.82 \cdot 10^{-5}$ mm^3/N/m, attributed to the presence of hardening phases within the coating's structure, compared to $38,24 \cdot 10^{-5}$ mm^3/N/m for the austenite-based coating.

References

1. Straffelini G., Bizzotto G., Zanon V. Improving the wear resistance of tools for stamping. *Wear*. 2010;269(9-10): 693—697. https://doi.org/10.1016/j.wear.2010.07.004
2. Ivanov V.I., Burumkulov F.Kh. Strengthening and increasing the service life of objects using the electrospark deposition method: classification, features of the technology. *Elektronnaya obrabotka materialov*. 2010;5:27—36. (In Russ.).
Иванов В.И., Бурумкулов Ф.Х. Упрочнение и увеличение ресурса объектов электроискровым методом: классификация, особенности технологии. *Электронная обработка материалов*. 2010;5:27—36.
3. Ivanov V.I. Increasing the service life of separation dies by strengthening and restoring them by electric spark alloying; Diss. Cand Sci. (Eng.). Saransk: VNIITUVID "Remdetal'", 2000. (In Russ.).
Иванов В.И. Повышение ресурса разделительных штампов путем упрочнения и восстановления их электроискровым легированием: Дис. ... канд. техн. наук. Саранск: ВНИИТУВИД «Ремдеталь», 2000.
4. Gadalov V.N., Gvozdev A.E., Starikov N.E., Romanenko D.N., Kalinin A.A., Filatov E.A., Makarova I.A., Vornacheva I.V. Increase of reliability of tooling and instrument of the stamping equipment. *Izvestiya Tul'skogo gosudarstvennogo universiteta. Tekhnicheskie nauki*. 2017;11(2):114—124. (In Russ.).
Гадалов В.Н., Гвоздев А.Е., Стариков Н.Е., Романенко Д.Н., Калинин А.А., Филатов Е.А., Макарова И.А., Ворначева И.В. Повышение надежности оснастки и инструмента штампового оборудования. *Известия Тульского государственного университета. Технические науки*. 2017;11(2):114—124.
5. Kudryashov A.E., Levashov E.A., Aksenov L.B., Petrov V.M. Use of electric spark alloying technology and promising nanostructured electrode materials for improving the life of punching equipment. *Metallurgist*. 2010;54(7):514—522.
Кудряшов А.Е., Левашов Е.А., Аксенов Л.Б., Петров В.М. Применение технологии электроискро-

вого легирования и перспективных наноструктурированных электродных материалов для повышения стойкости штамповой оснастки. *Металлург*. 2010;8:44—50.

6. Tušek J., Kosec L., Lešnjak A., Muhič T. Electrospark deposition for die repair. *Metalurgiya*. 2012;51:17—20.
7. Kuptsov K.A., Sheveyko A.N., Sidorenko D.A., Shtansky D.V. Electro-spark deposition in vacuum using graphite electrode at different electrode polarities: Peculiarities of microstructure, electrochemical and tribological properties. *Applied Surface Science*. 2021;566:150722.
https://doi.org/10.1016/j.apsusc.2021.150722
8. Kuptsov K.A., Antonyuk M.N., Sheveyko A.N., Shtansky D.V. Hydrophobic, anti-ice, wear- and corrosion-resistant C—(Ti)—PTFE coatings on Ti obtained by electrospark deposition using PTFE-impregnated graphite electrode. *Surface and Coatings Technology*. 2023;465:129621.
https://doi.org/10.1016/j.surfcoat.2023.129621
9. Kudryashov A.E., Kiryukhantsev-Korneev P.V., Mukanov S.K., Petrzhik M.I., Levashov E.A. The effect of electrospark deposition using zirconium electrodes on structure and properties of nickel-containing alloy obtained selective laser melting. *Powder Metallurgy and Functional Coatings*. 2022;3:63—77. (In Russ.).
https://doi.org/10.17073/1997-308X-2022-3-63-77
Кудряшов А.Е., Кирюханцев-Корнеев Ф.В., Муканов С.К., Петржик М.И., Левашов Е.А. Влияние электроискровой обработки электродами из циркония на структуру и свойства никельсодержащего сплава, полученного селективным лазерным сплавлением. *Известия вузов. Порошковая металлургия и функциональные покрытия*. 2022;3:63—77.
https://doi.org/10.17073/1997-308X-2022-3-63-77
10. Tarelnyk V.B., Paustovskii A.V., Tkachenko Y.G., Konoplianchenko E.V., Martsynkovskyi V.S., Antoszewski B. Electrode materials for composite and multilayer electrospark-deposited coatings from Ni—Cr and WC—Co alloys and metals. *Powder Metallurgy and Metal Ceramics*. 2017;55:585—595.
https://doi.org/10.1007/s11106-017-9843-2
11. Mukanov S.K., Baskov F.A., Petrzhik M.I., Levashov E.A. Electro-spark treatment with low-melting Al—Si and Al—Ca electrodes in order to improve wear and oxidation resistance of EP741NP alloy prepared by selective laser melting. *Metallurgist*. 2022;66:317—326.
https://doi.org/10.1007/s11015-022-01331-0
12. Renna G., Leo P., Casalino G., Cerri E. Repairing 2024 aluminum alloy via electrospark deposition process: A feasibility study. *Advances in Materials Science and Engineering*. 2018:8563054.
https://doi.org/10.1155/2018/8563054
13. Kandeva M., Kostadinov G., Penyashki T., Kamburov V., Petrzhik M., Elenov B., Nikolov A., Dimitrova R., Valkanov S. Abrasive wear resistance of electrospark coatings on titanium alloys. *Tribology in Industry*. 2022; 44:132—142.
https://doi.org/10.24874/ti.1143.06.21.09
14. Kostadinov G., Danailov P., Dimitrova R., Kandeva M., Penyashki T., Kamburov V., Nikolov A., Elenov B. Surface topography and roughness parameters of electrospark coatings on titanium and nickel alloys. *Applied Engineering Letters Journal of Engineering and Applied Sciences*. 2021;6:89—98.
https://doi.org/10.18485/aeletters.2021.6.3.1
15. Burkov A., Pyachin S. Investigation of WC—Co electrospark coatings with various carbon contents. *Journal of Materials Engineering and Performance*. 2014;23: 2034—2042.
https://doi.org/10.1007/s11665-014-0974-z
16. Burkov A., Pyachin S. Formation of WC—Co coating by a novel technique of electrospark granules deposition. *Materials & Design*. 2015;80:109—115.
https://doi.org/10.1016/j.matdes.2015.05.008
17. Barile C., Casavola C., Pappalettera G., Renna G. Advancements in electrospark deposition (ESD) technique: A short review. *Coatings*. 2022;12:1536.
https://doi.org/10.3390/coatings12101536
18. Kuz'min M.P., Chu P.K., Qasim A.M., Larionov L.M., Kuz'mina M.Yu., Kuz'min P.B. Obtaining of Al—Si foundry alloys using amorphous microsilica — Crystalline silicon production waste. *Journal of Alloys and Compounds*. 2019;806:806—813.
https://doi.org/10.1016/j.jallcom.2019.07.312
19. Kuz'min M.P., Kuz'mina M.Yu., Kuz'min P.B. Possibilities and prospects for producing silumins with different silicon contents using amorphous microsilica. *Transactions of Nonferrous Metals Society of China*. 2020;30(5):1406—1418.
https://doi.org/10.1016/S1003-6326(20)65306-7
20. Chengyong W., Xie Y., Zheng L., Qin Z., Tang D., Song Y. Research on the chip formation mechanism during the high-speed milling of hardened steel. *International Journal of Machine Tools and Manufacture*. 2014;79:31—48.
https://doi.org/10.1016/j.ijmachtools.2014.01.002
21. Dvornik M.I., Mikhailenko E.A. Production of WC—15Co ultrafine-grained hard alloy from powder obtained by VK15 alloy waste spark erosion in water. *Powder Metallurgy and Functional Coatings*. 2020;(3):4—16. (In Russ.).
https://doi.org/10.17073/1997-308X-2020-3-4-16
Дворник М.И., Михайленко Е.А. Создание ультрамелкозернистого твердого сплава WC—15Co из порошка, полученного электроэрозионным диспергированием отходов сплава ВК15 в воде. *Известия*

вузов. Порошковая металлургия и функциональные покрытия. 2020;(3):4—16.
https://doi.org/10.17073/1997-308X-2020-3-4-16

22. Potanin A.Yu., Vorotilo S., Pogozhev Yu.S., Rupasov S.I., Lobova T.A., Levashov E.A. Influence of mechanical activation of reactive mixtures on the microstructure and properties of SHS-ceramics $MoSi_2$—HfB_2—MoB. *Ceramics International.* 2019;45(16):20354—20361.
https://doi.org/10.1016/j.ceramint.2019.07.009
23. Zamulaeva E.I., Sheveyko A.N., Kaplanskii Y.Y., Levashov E.A. Structure formation and tribological properties of Mo—Si—B—Hf electrospark coatings based on Mo_2Ni_3Si laves phase. *Materials.* 2022;15(16):5613.
https://doi.org/10.3390/ma15165613
24. Gitlevich A.E., Mikhailov V.V., Parkanskii N.Ya., Revutskii V.M. Electrospark deposition of metal surfaces. Kishinev: Shtiintsa, 1985. 196 p. (In Russ.).
Гитлевич А.Е., Михайлов В.В., Парканский Н.Я., Ревуцкий В.М. Электроискровое легирование металлических поверхностей. Кишинев: Штиинца, 1985. 196 с.
25. Nan Chen, Ren Luo, Huiwen Xiong, Zhiyou Li. Dense M2 high speed steel containing core-shell MC carbonitrides using high-energy ball milled M2/VN composite powders. *Materials Science and Engineering: A.* 2020:771(138628).
https://doi.org/10.1016/j.msea.2019.138628
26. Verkhoturov A.D., Podchernyaeva I.A., Pryadko L.F., Egorov F.F. Electrode materials for electrospark deposition. Moscow: Nauka, 1988. 200 p. (In Russ.).
Верхотуров А.Д., Подчерняева И.А., Прядко Л.Ф., Егоров Ф.Ф. Электродные материалы для электроискрового легирования. М.: Наука, 1988. 200 с.
27. Huyan F., Larker R., Rubin P. Effect of solute silicon on the lattice parameter of ferrite in ductile irons. *ISIJ International.* 2014;54:248—250.
https://doi.org/10.2355/isijinternational.54.248
28. Phase equilibrium diagrams of binary metal systems: Directory. Vol. 2. Ed. N.P. Lyakishev. Moscow: Mashinostroenie, 1997. 1024 p. (In Russ.).
Диаграммы состояния двойных металлических систем: Справочник. В 3 т. Т. 2. Под общ. ред. Н.П. Лякишева. М.: Машиностроение, 1997. 1024 с.
29. Phase equilibrium diagrams of binary metal systems: Directory. Vol. 3. Book 1. Ed. N.P. Lyakishev. Moscow: Mashinostroenie, 2001. 872 p. (In Russ.).
Диаграммы состояния двойных металлических систем: Справочник. В 3 т. Т. 3. Кн. 1. Под общ. ред. Н.П. Лякишева. М.: Машиностроение, 2001. 872 с.
30. Ozden M.G., Morley N.A. Laser additive manufacturing of Fe-based magnetic amorphous alloys. *Magnetochemistry.* 2021;7:20.
https://doi.org/10.3390/magnetochemistry7020020
31. Fakoori Hasanabadi M., Malek Ghaini F., Ebrahimnia M., Shahverdi H.R. Production of amorphous and nanocrystalline iron based coatings by electro-spark deposition process. *Surface and Coatings Technology.* 2015;270:95—101.
https://doi.org/10.1016/j.surfcoat.2015.03.016
32. Hamaguchi T., Nakamura R., Asano K., Wada T., Suzuki T. Diffusion of boron in an amorphous iron-boron alloy. *Journal of Non-Crystalline Solids.* 2023; 601:122070.
https://doi.org/10.1016/j.jnoncrysol.2022.122070

Information about the authors

Amankeldy Akhmetov – Engineer of Scientific Project of the Department of Powder Metallurgy and Functional Coatings (PM&FC), National University of Science and Technology "MISIS" (NUST MISIS).
https://orcid.org/0000-0002-1606-838X
E-mail: aman1aotero@gmail.com

Zhanna V. Eremeeva – Dr. Sci. (Eng.), Professor of the Department of PM&FC, NUST MISIS.
https://orcid.org/0000-0002-1790-5004
E-mail: eremeeva-shanna@yandex.ru

Alexander E. Kudryashov – Cand. Sci. (Eng.), Leading Researcher at the Laboratory "In Situ Diagnostics of Structural Transformations" of Scientific-Educational Center of SHS (SHS-Center) of MISIS–ISMAN.
https://orcid.org/0000-0001-6222-4497
E-mail: aekudr@yandex.ru

Информация об авторах

Аманкельды Ахметов – инженер научного проекта кафедры порошковой металлургии и функциональных покрытий (ПМиФП) Национального исследовательского технологического университета «МИСИС» (НИТУ МИСИС).
https://orcid.org/0000-0002-1606-838X
E-mail: aman1aotero@gmail.com

Жанна Владимировна Еремеева – д.т.н., профессор кафедры ПМиФП, НИТУ МИСИС.
https://orcid.org/0000-0002-1790-5004
E-mail: eremeeva-shanna@yandex.ru

Александр Евгеньевич Кудряшов – к.т.н., вед. науч. сотрудник лаборатории «In situ диагностика структурных превращений» Научно-учебного центра (НУЦ) СВС МИСИС–ИСМАН.
https://orcid.org/0000-0001-6222-4497
E-mail: aekudr@yandex.ru

Pavel A. Loginov – Cand. Sci. (Eng.), Senior Lecturer of the Department of PM&FC of NUST MISIS; Senior Research Scientist of the Laboratory "In situ Diagnostics of Structural Transformations" of SHS-Center of MISIS–ISMAN.
https://orcid.org/0000-0003-2505-2918
E-mail: pavel.loginov.misis@list.ru

Sergey D. Shlyapin – Dr. Sci. (Eng.), Professor of the Department of Materials Science and Materials Processing Technology, Moscow Aviation Institute (National Research University); Lead Project Expert of NUST MISIS.
https://orcid.org/0000-0002-1323-2623
E-mail: sshliapin@yandex.ru

Marina E. Samoshina – Cand. Sci. (Eng.), Head of the Division of Academic Degrees, Academic Secretary of NUST MISIS Dissertation Board.
https://orcid.org/0009-0000-2773-3122
E-mail: samoshina@list.ru

Evgeny A. Levashov – Dr. Sci. (Eng.), Prof., Academic of the Russian Academy of Natural Science, Head of the Department of PM&FC of NUST MISIS, Head of SHS-Center of MISIS–ISMAN.
https://orcid.org/0000-0002-0623-0013
E-mail: levashov@shs.misis.ru

Павел Александрович Логинов – к.т.н., ст. преподаватель кафедры ПМиФП НИТУ МИСИС; ст. науч. сотрудник лаборатории «In situ диагностика структурных превращений» НУЦ СВС МИСИС–ИСМАН.
https://orcid.org/0000-0003-2505-2918
E-mail: pavel.loginov.misis@list.ru

Сергей Дмитриевич Шляпин – д.т.н., профессор кафедры «Материаловедение и технология обработки материалов» Московского авиационного института (национального исследовательского университета); ведущий эксперт по проектам НИТУ МИСИС.
https://orcid.org/0000-0002-1323-2623
E-mail: sshliapin@yandex.ru

Марина Евгеньевна Самошина – к.т.н., начальник отдела ученых степеней, ученый секретарь диссертационного совета НИТУ МИСИС.
https://orcid.org/0009-0000-2773-3122
E-mail: samoshina@list.ru

Евгений Александрович Левашов – д.т.н., акад. РАЕН, профессор, зав. кафедрой ПМиФП НИТУ МИСИС; директор НУЦ СВС МИСИС–ИСМАН.
https://orcid.org/0000-0002-0623-0013
E-mail: levashov@shs.misis.ru

Contribution of the authors

A. Akhmetov – conducting experiments, manuscript writing.

Zh.V. Eremeeva – investigating consolidation features of powder mixtures, analyzing the microstructure of electrode materials, participating in result discussions.

A.E. Kudryashov – exploring electrospark deposition characteristics using the specified electrodes and analyzing the microstructure of the resulting coatings; participating in result discussions.

P.A. Loginov – conducting research using transmission electron microscopy.

S.D. Shlyapin – drafting and editing the manuscript, participating in the discussion of the results.

M.E. Samoshina – editing the manuscript, participating in result discussions.

E.A. Levashov – conceptualizing the research, contributed to the drafting and editing of the manuscript, and participated in the discussion of the findings.

Вклад авторов

А. Ахметов – проведение экспериментов, подготовка текста статьи.

Ж.В. Еремеева – исследование особенностей консолидации порошковых смесей, анализ микроструктуры электродных материалов, участие в обсуждении результатов.

А.Е. Кудряшов – исследование особенностей процесса электроискровой обработки рассматриваемыми электродами, анализ микроструктуры сформированных покрытий, участие в обсуждении результатов.

П.А. Логинов – исследование методом просвечивающей электронной микроскопии.

С.Д. Шляпин – составление и редактирование текста статьи, участие в обсуждении результатов.

М.Е. Самошина – редактирование текста статьи, участие в обсуждении результатов.

Е.А. Левашов – концептуализация проводимых исследований, составление и редактирование текста статьи, участие в обсуждении результатов.

The article was submitted 01.12.2023, revised 22.01.2024, accepted for publication 24.01.2024

Статья поступила в редакцию 01.12.2023, доработана 22.01.2024, подписана в печать 24.01.2024